Science Advances
AAAS

advances.sciencemag.org/cgi/content/full/5/5/eaav8965/DC1

Supplementary Materials for

Tracking ultrafast hot-electron diffusion in space and time by ultrafast thermomodulation microscopy

A. Block*, M. Liebel, R. Yu, M. Spector, Y. Sivan, F. J. García de Abajo, N. F. van Hulst*

*Corresponding author. Email: alexander.block@icfo.eu (A.B.); niek.vanhulst@icfo.eu (N.F.v.H.)

Published 10 May 2019, *Sci. Adv.* **5**, eaav8965 (2019)
DOI: 10.1126/sciadv.aav8965

This PDF file includes:

Note S1. General diffusion model
Note S2. Two-temperature model
Note S3. Thermo-optical response
Note S4. Calculation of the transient reflectivity
Fig. S1. Long-time dynamics of $\Delta R/R$.
Fig. S2. Scheme of thermo-optical calculations.
Fig. S3. Schematic of the SUTM setup.
Fig. S4. Different contributions to the thermo-optical response.
References (*45*–*57*)

Note S1. General diffusion model

As stated in the main text, we estimate diffusivity, or diffusion coefficient, in a first approximation from the slope of the FWHM^2 vs. time plot, before the more rigorous modeling described thereafter. Thus, to quantify a general diffusion process with a time-dependent diffusivity $D(t)$, we assume that the absorbed pump power induces a Gaussian energy distribution at the sample $u(\mathbf{x}, t = 0) \propto \exp\left(-4 \ln 2 \, |\mathbf{x}|^2 / \mathrm{FWHM}_{\mathrm{pump}}^2\right)$, where $\mathbf{x} \in \mathbb{R}^n$ (n = 1,2, or 3, spatial dimension) and that u evolves according to a heat equation (*33*)

$$\frac{\partial u(\mathbf{x},t)}{\partial t} = D(t) \nabla^2 u(\mathbf{x}, t) \tag{S1}$$

or, alternatively, a heat equation including a decay with a rate $\Gamma = 1/\tau$

$$\frac{\partial u(\mathbf{x},t)}{\partial t} = D(t) \nabla^2 u(\mathbf{x}, t) - \Gamma \, u(\mathbf{x}, t) \tag{S2}$$

Interestingly, both solutions of $u(\mathbf{x}, t)$ to equations S1 and S2 are temporally decaying spatial Gaussian profiles with a time-dependent width. The full-width at half-maximum, measured in any one dimension, $\mathrm{FWHM}(t)$, is related to $D(t)$ via

$$\frac{\partial \mathrm{FWHM}^2(t)}{\partial t} = 16 \ln 2 \, D(t) \tag{S3}$$

This result is the generalization of the more common result known for a time-independent diffusivity D, $\sigma^2(t) = \sigma^2(0) + 2\,D \cdot t$, and converting the Gaussian width parameter σ to FWHM using $\mathrm{FWHM} = 2\sqrt{2 \ln 2}\,\sigma$.

Under the assumption that our observed profiles $\Delta R/R(\mathbf{x}, t)$ scale linearly with $u(\mathbf{x}, t)$, we can determine $D(t)$ from our space-time-resolved data. We note that this derivation is often shown for the n-dimensional mean square displacement $\langle \mathbf{x}^2 \rangle$, which is dependent on the dimensionality n, yet the projection onto one axis, or a 1D "cutline" of the profile, is independent of n.

Note S2. Two-temperature model

In this model, the electron and lattice temperature T_e and T_l are assumed to be time- and position-dependent, with their spatio-temporal behavior being described by the following coupled equations (*31*)

$$C_e(T_e) \frac{\partial T_e}{\partial t} = \nabla(k_e(T_e) \, \nabla T_e) - G(T_e - T_l) + S - S_{es} \tag{S4a}$$

$$C_l \frac{\partial T_l}{\partial t} = \nabla(k_l \, \nabla T_l) + G(T_e - T_l) - S_{ls} \tag{S4b}$$

$$C_s \frac{\partial T_s}{\partial t} = \nabla(k_s \, \nabla T_s) + S_{ls} + S_{es} \tag{S4c}$$

with $C_e(T_e) = \gamma T_e$, $\gamma = 71$ $Jm^{-3}K^{-2}$, for the electron heat capacity (*27*) ; $C_l = 2.45 \cdot 10^6$ Jm^{-3} K^{-1} for the lattice heat capacity (*37*); $k_e(T_e, T_l) = k_0 T_e / T_l$, with $k_0 = 317$ $Wm^{-1}K^{-1}$, for the electron thermal conductivity (*27*); $k_l = 2.6$ $Wm^{-1}K^{-1}$, for the lattice thermal conductivity (*38*); $C_s = 1.848 \cdot 10^6$ Jm^{-3} K^{-1} for the glass substrate heat capacity (*40*) ; $k_s = 0.8$ $Wm^{-1}K^{-1}$ for the substrate thermal conductivity (*40*) ; $G = 2.2 \cdot 10^{16}$ $Wm^{-3}K^{-1}$ for gold electron-phonon coupling coefficient (*39*); $S_{es/ls} = G_{es/ls}(T_{e/l} - T_s)$ represents the boundary interface heat exchange between the gold electron/lattice and the glass substrate, where $G_{es} = (96.12 + 0.189T_e)$ $MWm^{-2}K^{-1}$ and $G_{ls} = 141.5$ $MWm^{-2}K^{-1}$ are the corresponding thermal boundary conductance, respectively (*34*). In Eq. S4a, the source term is defined for a Gaussian beam excitation as (*45*)

$$S(\mathbf{r}, t) = \frac{S_a}{\delta} F \cdot \exp\left[-\frac{z}{\delta} - (4\ln 2)\frac{x^2+y^2}{\mathrm{FWHM}_{\mathrm{pump}}^2}\right] \cdot \frac{1}{t_{\mathrm{pump}}}\sqrt{\frac{4\ln 2}{\pi}} \exp\left[-(4\ln 2)\frac{(t-2t_{\mathrm{pump}})^2}{t_{\mathrm{pump}}^2}\right] \qquad \text{(S5)}$$

with a full-width at half-maximum $\mathrm{FWHM}_{\mathrm{pump}} = 0.6\ \mu\mathrm{m}$, and a pulse duration $t_{\mathrm{pump}} = 0.2$ ps. The absorbance $S_a = 1 - R - T = 0.5$ and the penetration depth $\delta = 18.7\ \mathrm{nm}$ are estimates based on tabulated optical data for gold at the pump wavelength of 450 nm (*41*), with R and T being the thin film reflectivity and transmissivity, respectively. *F* is the pump laser fluence. Note that the z=0 plane indicates the air-gold interface.

Note S3. Thermo-optical response

Here, we describe the model used to describe the electron and lattice temperature dependence of the permittivity (or dielectric function) ε.

The dielectric function of the gold film as a function of electron and lattice temperature at the probe wavelength (λ_{probe} = 900 nm) is well described by the Drude model (*41*), in which electrons are considered as free charges moving in response to an optical field oscillating at angular frequency ω. Using a classical equation of motion, the dielectric response of the plasma was shown to be

$$\varepsilon_{\mathrm{intra}} = \varepsilon_\infty - \frac{{\omega_p}^2(T_l)}{\omega(\omega + i\gamma_{re}(T_e, T_l))} \qquad \text{(S6)}$$

with the plasma frequency $\omega_p(T_l)$ being

$$\omega_p(T_l) = \sqrt{\frac{e^2}{\epsilon_0 m_{\mathrm{eff}}} \cdot n_e(T_l)} \qquad \text{(S7)}$$

Here, *e* is the electron charge; n_e is the free electron density in the conduction band (n_e= $5.9 \cdot 10^{22}$ cm^{-3} for Au (*42*)); ϵ_0 is the dielectric permittivity of the vacuum; m_{eff} is the effective mass (estimated as equal to the electron mass, m_e); and γ_{re} represents the total rate of collisions that conserve the total momentum and/or energy of the electron subsystem, i.e., collisions that cause relaxation of the electron system (in contrast to like regular e-e collisions, which affect the permittivity only indirectly, by causing a thermalization, i.e., a temperature increase). It is given by

$$\gamma_{re}(T_e, T_l) = \gamma_{e-ph}(T_l) + \gamma_{e-e}^{Um}(T_e) \quad \text{(S8)}$$

where the subscript re stands for relaxation, γ_{e-ph} is the electron-phonon (e-ph) collision rate and γ_{e-e}^{Um} is the Umklapp electron-electron (e-e) collision rate.

ε_∞ represents the off-resonant (i.e., high frequency) contribution of the interband transitions (ε_∞ = 9.5 for Au (*41*)). Here, we neglect its dependence on the temperatures which, according to recent results (*46*, *47*), is weak at the 900 nm probe wavelength. In addition, note that for $1200\ K \gg T_e > T_{\mathrm{Debye}}$, $T_l \approx 300\ K$, one can neglect the temperature dependence of m_{eff} (*48*). Thus, heating of a metal affects the intraband contribution to the dielectric constant only via two parameters, the plasma frequency ω_p and the constituents of the electron relaxation rate γ_{re}. We now specify in detail the temperature dependence of these parameters. The e-ph scattering rate, γ_{e-ph}, is given by $\gamma_{e-ph}(T_l) = B\ T_l$, where for Au, $B \approx 1.45 \cdot 10^{11}$ $K^{-1}s^{-1}$ (*43*).

γ_{e-e}^{Um} represents the intraband transition rate due to Umklapp e-e scattering events. In *normal e-e* scattering, the momentum is conserved so that it does not contribute directly to the intraband collision rate, γ_{re}. However, these collisions do cause the electron system to thermalize, hence, the electron temperature to increase, so that they contribute to the permittivity indirectly through the temperature dependence of other quantities in Eq. S6. *Umklapp e-e* scattering processes, however, impart momentum to the lattice as a whole, thus, the total electron momentum is not conserved, whereas the quantity that is conserved is the quasi-momentum. Violation of momentum conservation leads to contribution to the collision rate (*49*). As shown by Kaveh and Wiser (*50*), within the framework of Fermi Liquid Theory (*51*), it equals the fraction $\Delta^{(Um)}$ of the total e-e scattering rate, γ_{e-e}, i.e.

$$\gamma_{e-e}^{Um}(T_e) = \Delta^{(Um)}\gamma_{e-e} \quad \text{(S9)}$$

where $\gamma_{e-e} = AT_e^2$, and $A = K(\pi k_B)^2/2$. $K = m_e^3 W_{e-e}/(8\pi\hbar^6)$ is the characteristic e-e scattering constant that contains the angular-averaged scattering probability W_{e-e} (*51*); k_B is the Boltzmann constant. For Au, $A \approx 1.7 \cdot 10^7$ $K^{-2}s^{-1}$ (*43*) and $\Delta^{(Um)} \approx 0.77$ (*44*). Thus, γ_{e-e}^{Um} depends quadratically on T_e (*52*).

The plasma frequency is affected by the temperature rise via a change of n_e due to volume expansion of the metallic system (*53*). For the near-infrared probe wavelength, one can safely neglect the possibility of the density of the electrons in the conduction band to increase due to interband transitions. The volume reads

$$V(T_l) = V_{eq}(1 + \beta\Delta T_l) \quad \text{(S10)}$$

where V_{eq} is the equilibrium volume of the metallic system at ambient temperature T_0 and β is the volume thermal expansion coefficient. The thermal expansion coefficient is directly related to the Gruneisen constant γ_G according to the following equation (*54*): $\beta \approx \gamma_G C_l/B_b$, where B_b is the bulk modulus. Inserting the values for γ_G and B_b for Au (*55*), the thermal expansion coefficient is estimated

as $\beta = 4.23 \cdot 10^{-5}$ K^{-1}. We assume that the total number of electrons in the conduction band, N_e, is independent of temperature

$$N_e = n_e(T_0)V_{eq} \approx n_e(T_l)\mathrm{V}(T_l) \tag{S11}$$

so that the density is given by

$$n_e(T_l) = \frac{n_e(T_0)}{1+\beta\Delta T_l} \tag{S12}$$

Substitution of Eq. S12 in Eq. S7 leads to (*53*, *56*)

$$\omega_p(T_l) = \frac{\omega_p(T_0)}{\sqrt{1+\beta\Delta T_l}} \tag{S13}$$

or

$$\omega_p(T_l) = \sqrt{\frac{e^2}{\epsilon_0 m_{eff}} \cdot \frac{n_e(T_0)}{1+\beta\Delta T_l}} \tag{S14}$$

The dynamics of the change to the metal permittivity ensuing from the temperature dependence obtained from Eqs. S4 and Eqs. S6 - S11 are seen in Suppl. Fig. S4. One can see that the change of the imaginary part of the metal permittivity is much bigger than the change of the real part. Indeed, it can be shown that the observed increase of $\mathrm{Im}(\Delta\varepsilon_{\mathrm{intra}})$ causes the reflectivity to decrease; this explains the decrease-increase pattern observed in Fig. 2B and Suppl. Fig 2.

Another interesting observation is that the contribution to the change of the permittivity from the lattice heating becomes dominant over the contribution from the electron heating much earlier than the stage when the electron temperature cools down to the lattice temperature (i.e., for $T_e \gg T_l$). This happens because the derivative of the metal permittivity with respect to T_l is much higher than with respect to T_e.

Note S4. Calculation of the transient reflectivity

From the spatiotemporal maps of $T_e(\mathbf{x}, t)$ and $T_l(\mathbf{x}, t)$, we first calculate the reflectivity $R(T_e, T_l)$, and then the transient reflectivity $\Delta R/R = [R(T_e, T_l) - R(T_0, T_0)]\,/R(T_0, T_0)$. We use the thin-film Fresnel equations (*58*) for the reflection by a thin film (thickness h, refractive index $n_2 = \sqrt{\varepsilon}$ for gold (*41*)) under perpendicular incidence from air (n_1 = 1), with the film supported on a glass substrate (n_3 = 1.5)

$$R = |r|^2, \text{ with } r = \frac{r_{12}+r_{23}\cdot\exp(2i\beta)}{1+r_{12}\cdot r_{23}\cdot\exp(2i\beta)} \tag{S15}$$

where $\beta = 2\pi n_2 h/\lambda_0;\ r_{12} = (n_1 - n_2)/(n_1 + n_2);\ r_{23} = (n_2 - n_3)/(n_2 + n_3)$.

We note that as an alternative approach, we have also calculated R from finite z-slices of the 3D permittivity $\varepsilon(x, y, z)$, extracted directly from the 3D finite element method calculation mesh $T_e(x, y, z)$ and $T_l(x, y, z)$, using the transfer matrix method. As this calculation yielded nearly the same results as the simpler version (Eq. S15, assuming homogeneous permittivity along the film thickness z), we trust the validity of this approach.

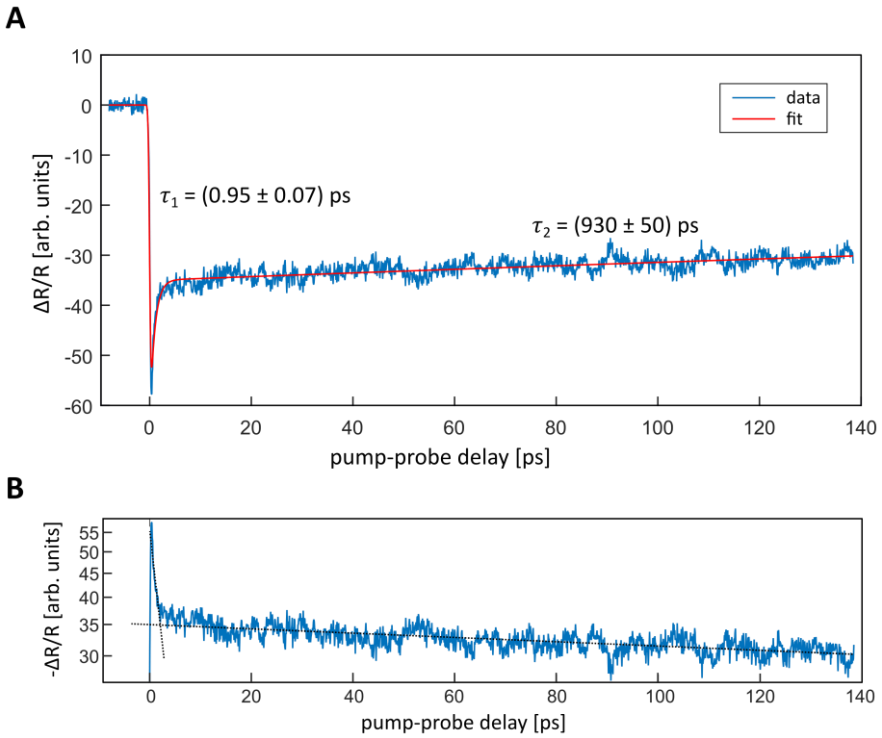

Fig. S1. Long-time dynamics of Δ*R*/*R*. This is an extension of Fig. 2B from the main text. (**A**) The red line shows the biexponential fit to extract the two decay parameters, where errors are 68 % confidence intervals. (**B**) Same as A, on linear-log scale. Dashed lines show the exponential decay parameters taken from the above fit.

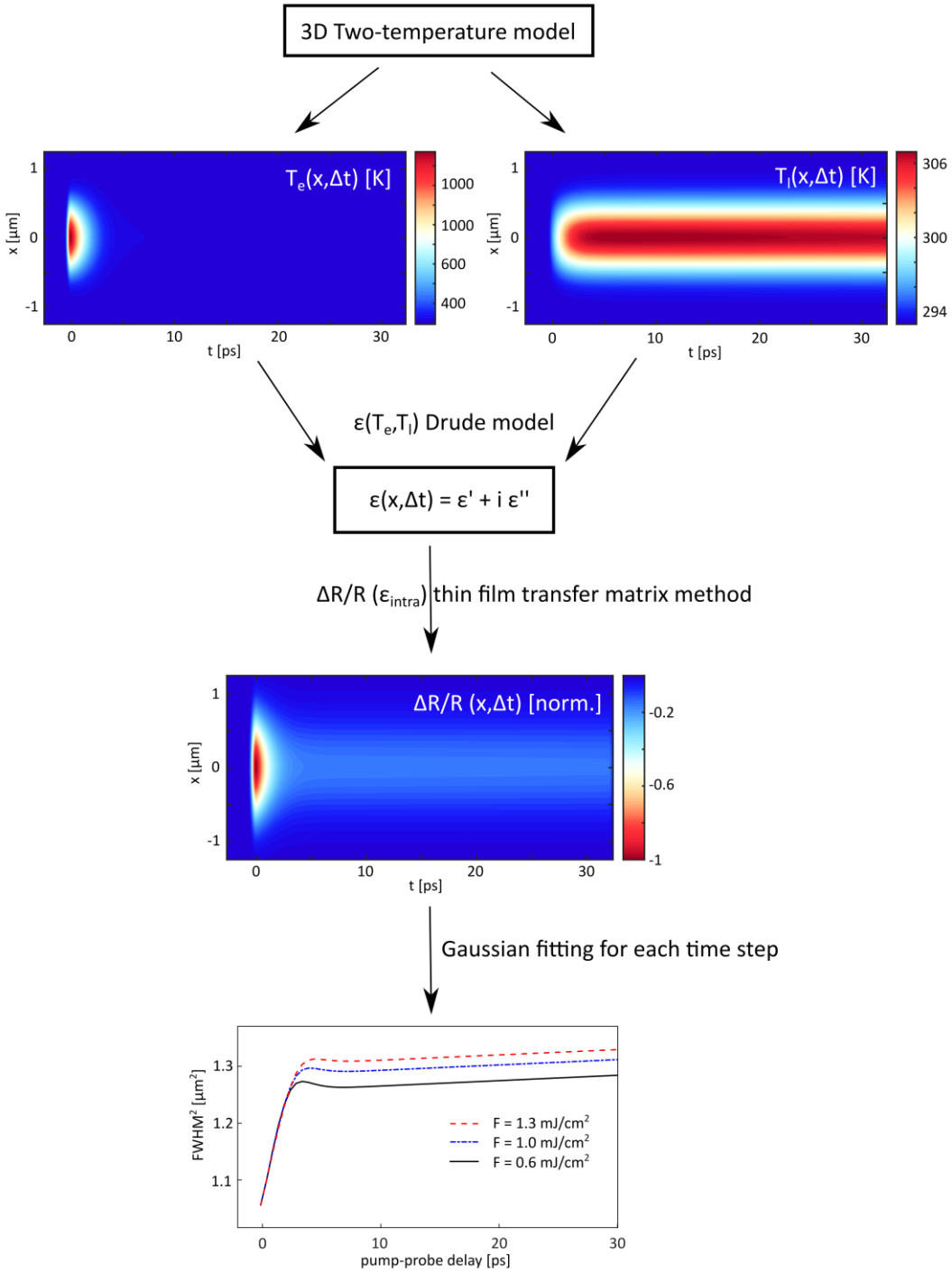

Fig. S2. Scheme of thermo-optical calculations. We calculate the temporal evolution of the spatial temperature profiles for the electron and lattice subsystems after optical excitation. Next, we calculate the spatio-temporal permittivity from the two-temperature maps using a temperature dependent Drude model described in Note S3. Finally, we convert the resulting permittivity to a transient reflectivity using the Fresnel coefficients for thin films (see Note S4). The evolution of the spatial width is calculated by fitting the $\Delta R/R$ maps to Gaussians.

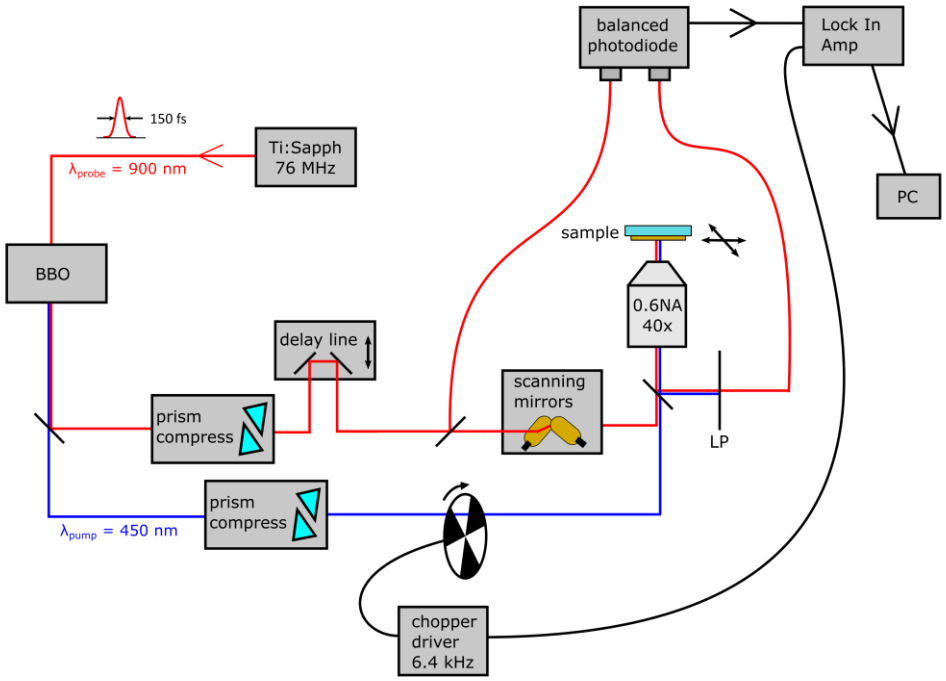

Fig. S3. Schematic of the SUTM setup. BBO: β-Barium borate crystal. The polarization of both pump and probe beams are linear and in the same plane. Both beams enter the objective with perpendicular angle of incidence with respect to the sample plane. The sample consists of a glass substrate (facing up) and air below the evaporated gold surface. Further description of the experiment is found in the main text.

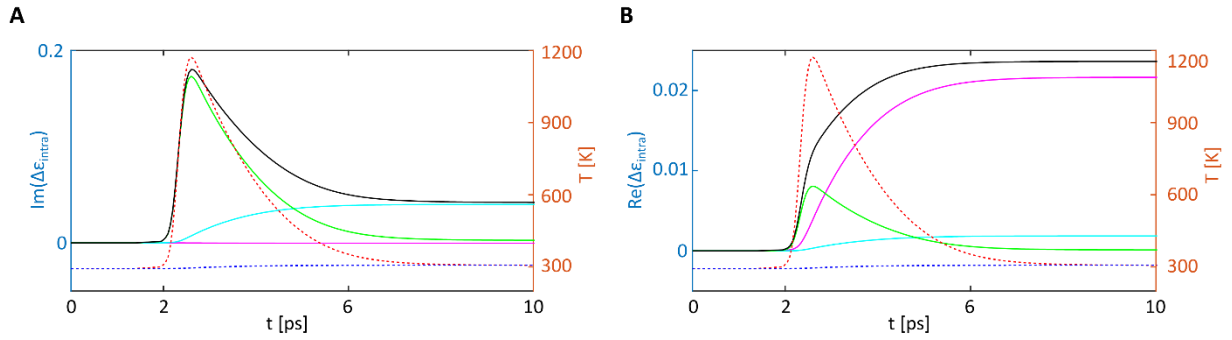

Fig. S4. Different contributions to the thermo-optical response. Both graphs show the temporal dynamics of the electronic and lattice temperatures (dashed red and blue lines, respectively). We show the corresponding dynamics of the (**A**) imaginary and (**B**) real parts of the metal permittivity change $\Delta\varepsilon_{intra}$ for λ_{probe} = 900nm. Umklapp e-e scattering, e-ph scattering, volume thermal expansion and the sum of the effects are represented respectively by green, cyan, magenta and black solid curves.